


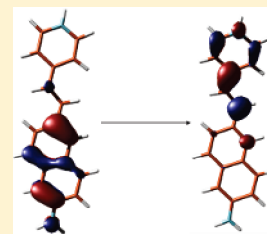
Di-8-ANEPPS Emission Spectra in Phospholipid/Cholesterol Membranes: A Theoretical Study

David Robinson,[†] Nicholas A. Besley,[†] Paul O'Shea,[‡] and Jonathan D. Hirst^{*,†}

[†]School of Chemistry and [‡]School of Biology, University of Nottingham, University Park, Nottingham, NG7 2RD, United Kingdom

 Supporting Information

ABSTRACT: We have investigated the effects of explicit molecular interactions and the membrane dipole potential on the absorption and emission spectra of a widely used fluorescent probe, di-8-ANEPPS, in a dipalmitoylphosphatidylcholine (DPPC) and a mixed DPPC/cholesterol membrane bilayer. Ground-state and excited-state geometries were calculated with the complete active space self-consistent field (CASSCF) method. Interactions with up to 260 atoms of the membrane bilayer were explicitly incorporated using a decoupled quantum mechanics/molecular mechanics (QM/MM) approach, utilizing recent advances in time-dependent density functional theory (TDDFT). We find that no specific molecular interactions affect the fluorescence of di-8-ANEPPS; rather, the magnitude of the membrane dipole potential is key to the shifts observed in both of the two lowest excited states.



INTRODUCTION

Molecular probes are useful in the study of properties of large biological systems.^{1–10} Most biomolecules possess few natural moieties with exploitable optical properties, and therefore, the strategy of extrinsic labeling with spectroscopic probes is often employed. For example, green fluorescent protein (GFP) is widely used with great success.^{1–6} However, at 238 amino acids in size, it may affect normal biological function in some systems, and therefore, other fluorescent molecules have found use, especially in phospholipid membrane systems.^{11–19}

Cell membranes play an active role in the selective trafficking of molecules into and out of cells. The mechanism by which this occurs is not fully understood, but the electrostatic potential, Ψ , across the membrane seems to be of critical importance.^{20–24} The difference in potential, $\Delta\Psi$, across a membrane arises from different concentrations of anions and cations in the bulk phases on either side of the membrane. For membranes containing lipids with charged head groups, there is a surface potential, Ψ_s , which controls the concentration of any ions found near the membrane surface. Within the membrane interior, there is an alignment of the dipole moments of the lipid head groups and the water molecules, leading to the formation of a dipole potential, Ψ_d .²⁰ These potentials all contribute to the total electrostatic potential of the membrane.

The aminonaphthylethylpyridinium (ANEP) class of dyes (Figure 1) are one of a few fast potentiometric membrane probes that can yield fluorescence shifts in response to changes in Ψ_d in the submillisecond regime.^{11–19} This is predicated on the fluorescence shifts only being affected by the dipole potential and not also by specific molecular interactions. Experimental evidence shows that only the potential due to the ordering of the dipole moments and not the surface potential causes fluorescence shifts. Evidence of the role of explicit molecular interactions has been explored experimentally.¹⁹ From the authors' observation of a linear Lippert plot, with none of the solvents

showing a significant deviation from the line, they were able to conclude that there was no evidence for any specific interactions between the dye and these solvents. In light of this, and to ameliorate the effect of different concentrations of the probe in different samples, the ratio of the measured intensity of the first emissive state, excited from two different wavelengths, is taken, and it is the difference in these ratios between different systems that is used to measure the dipole potential. A novel technique to increase the sensitivity of the ANEP dyes is gaining popularity. This involves second harmonic generation (SHG), a nonlinear optical effect.^{11,12,16,17}

There are few theoretical investigations of the electronic spectra of di-8-ANEPPS. Clark et al.²⁵ studied the SHG of di-8-ANEPPS using a combined quantum mechanics/molecular mechanics (QM/MM) approach. Semiempirical configuration interaction (CI) was employed to account for the electronically excited states of di-8-ANEPPS, while the rest of the membrane system was treated as point charges that interact with the electronic wave function via a one-electron term in the Hamiltonian. This study gave a qualitatively solid description of the SHG spectrum of di-8-ANEPPS and the influence of the membrane dipole potential upon it but did not study the influence of specific explicit molecular interactions.

Complete active space self-consistent field (CASSCF)²⁶ and multireference perturbation theory (CASPT2)^{27–30} calculations using implicit solvent models, such as the polarizable continuum model (PCM),³¹ allow for detailed electronic description of the bulk solvent effect on the excited states of interest. Using cheaper time-dependent density functional theory (TDDFT) calculations, absorption spectra can be readily computed, incorporating explicitly large portions of the environment surrounding the

Received: November 22, 2010

Revised: January 31, 2011

Published: March 22, 2011

chromophore. We have previously calculated absorption and emission spectra for 5-hydroxyindole in solution,³² showing the critical importance of intermolecular bonds between the solute and solvent on the spectra. We also calculated the spectra for 5-hydroxytryptophan in six different protein environments,³³ again highlighting the importance of including explicit molecular interactions within calculations of excited states of fluorophores. In both cases, CASSCF geometry optimizations of the electronically excited states provided a route for the calculation of fluorescence, and TDDFT calculations were used to characterize the electronic excited states.

In the present paper, we study the effects of the explicit molecular interactions of di-8-ANEPPS in dipalmitoylphosphatidylcholine (DPPC) membranes, and membranes with 30% molar concentration of cholesterol, and also the effect of the dipole potential. Taking snapshots from classical molecular dynamics (MD) simulations allows for the inclusion of thermal broadening effects. We also rationalize the effect of the dipole potential on the fluorescence shifts of the first excited state, and also of the second excited state, which is less than 1 eV higher in energy for the Franck–Condon excitation.

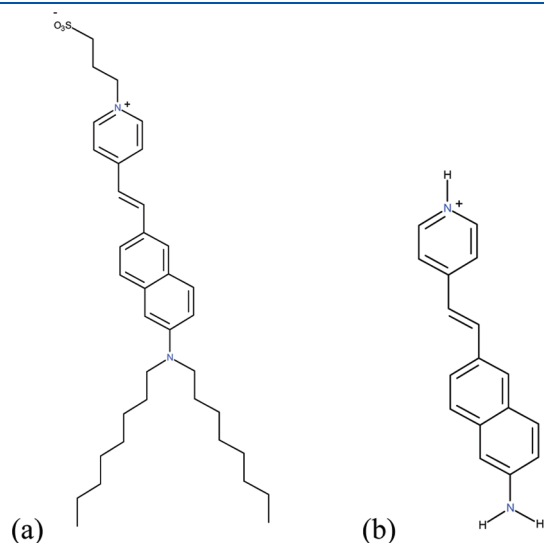


Figure 1. (a) Di-8-ANEPPS (used in the molecular dynamics simulations in this work). (b) The truncated model of di-8-ANEPPS used in the electronic structure calculations in this work.

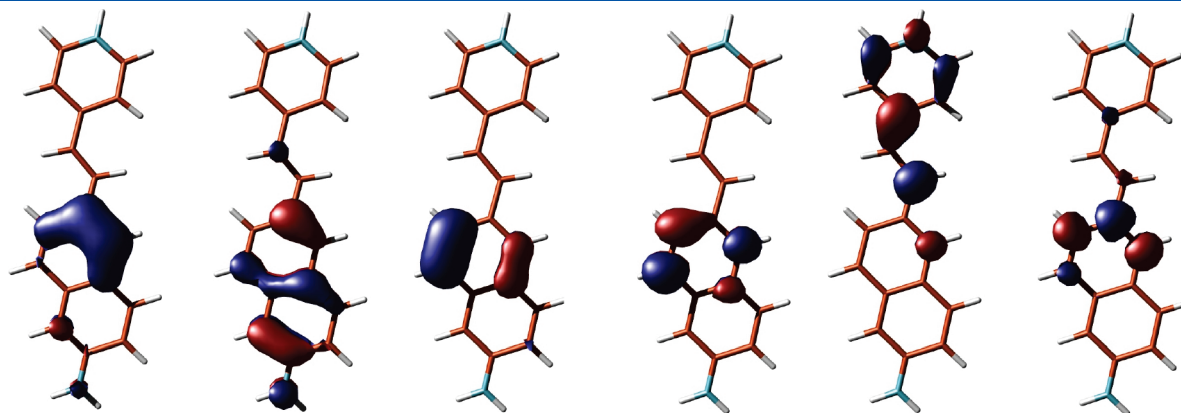


Figure 2. Active space molecular orbitals obtained from the CASSCF calculations. From left to right (with indices used in this work in parentheses): 8a'' (1), 9a'' (2), 10a'' (3), 12a'' (4), 15a'' (5), 16a'' (6).

THEORETICAL DETAILS

Gas-phase ground- and excited-state geometries (provided in the Supporting Information) were obtained at the CASSCF level of theory, using the atomic natural orbital (ANO-L) basis set,³⁴ contracted to 4s3p2d for heavy atoms and 2s1p for hydrogen.

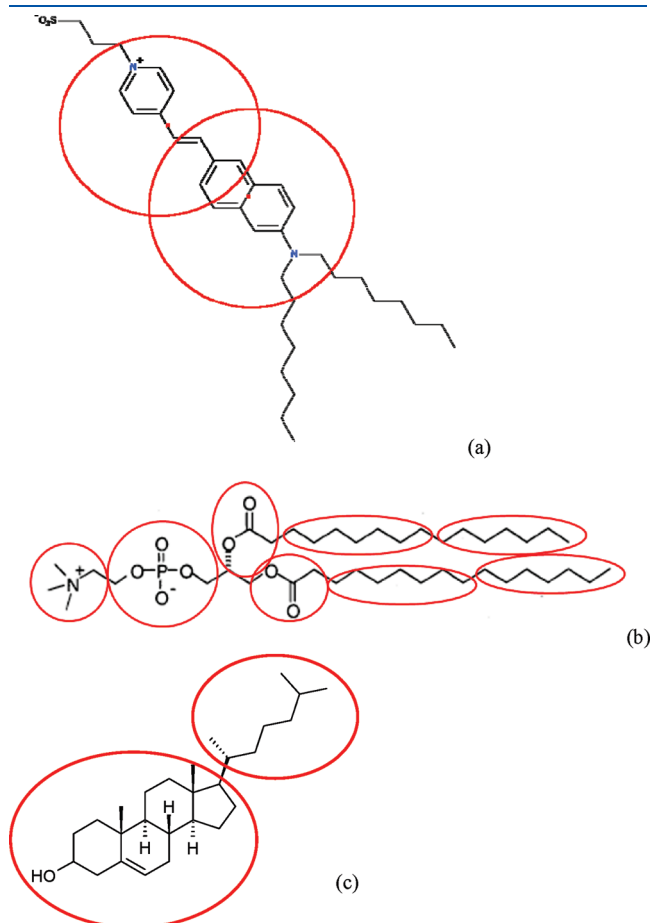


Figure 3. (a) Distance criteria from di-8-ANEPPS for lipids to be included in the explicit TDDFT (LRC-PBE) calculation (circles have a radius of 4.5 Å). (b) Subgroups of the DPPC lipid that are used within the TDDFT calculations, to avoid intractable numbers of atoms being included. (c) Corresponding subgroups of cholesterol included within the TDDFT calculations explicitly.

Table 1. Leading Electronic Configurations for the First Three States of Di-8-ANEPPS at the Relaxed Geometry, Calculated at the CASSCF (6,6)/ANO-L (C,N,O 4s3p1d; H 2s1p) Level of Theory^a

electronic state	determinant(s)	dipole moment/debye	CI coefficient	% of CASSCF wave function
GS	1̄12̄2̄3̄3̄>	14.9	0.95	91
1A'	1̄12̄3̄3̄5̄>	3.4	0.90	81
	1̄12̄2̄3̄3̄>		0.28	8
2A'	1̄12̄2̄3̄5̄>	3.9	0.80	64
	1̄12̄3̄3̄6̄>		−0.48	23

^a Numbers in the determinant refer to the active orbital that is occupied (Figure 1). A bar above a number refers to beta spin electrons. The CI coefficient is equivalent to a configuration coefficient.

Table 2. Natural Orbital Occupation Numbers for the First Three Electronic States of Di-8-ANEPPS at the Relaxed Geometry, Calculated at the CASSCF (6,6)/ANO-L (C,N,O 4s3p1d; H 2s1p) Level of theory

state	active space orbital					
	1	2	3	4	5	6
GS	1.96	1.93	1.91	0.09	0.03	0.07
1A'	1.94	1.40	1.90	0.10	0.60	0.06
2A'	1.94	1.90	1.04	0.04	0.98	0.09

An active space of six electrons in six orbitals (6,6) (see Figure 2) was determined from restricted active space self-consistent field calculations (RASSCF),³⁵ in which the full π system of 20 electrons in 19 orbitals (20,19) was used. Only the RAS1 and RAS3 subspaces were used, with a limit of single and double excitations from the occupied active orbitals into the unoccupied virtual orbitals. All CASSCF, CASPT2, and RASSCF calculations were performed with the Molcas program.³⁶

MD simulations were performed with the CHARMM software³⁷ and the CHARMM27 all-atom lipid force field.³⁸ The parameters for di-8-ANEPPS were derived from previous parameters for naphthalene,³⁹ pyridine,⁴⁰ and 2,3-butene.³⁸ The parameters are available in the Supporting Information. The system consisted of a bilayer of 100 DPPC lipids (50 in each leaflet), each chosen at random from a library of 2000 pre-equilibrated DPPC lipids (each has one to eight primary water molecules). Bulk solvent was added to each leaflet to give a total of 3416 TIP3P water molecules.⁴¹ Di-8-ANEPPS was added to the membrane on the upper leaflet (defined as having positive values for the coordinates with respect to the membrane normal). The SHAKE algorithm⁴² was used for all bonds involving hydrogen. The nonbonded interactions were truncated at 12 Å using a switching function starting at 10 Å, and the long-range electrostatics were treated using particle mesh Ewald summations.⁴³ Initially, harmonic constraints were imposed on the lipid and water molecules to allow the system to properly equilibrate. The constraints were gradually reduced until the final 5 ps of equilibration, where constraints were totally removed. The total system was minimized using the adapted basis Newton–Raphson algorithm and was equilibrated by Langevin dynamics for 30 ps at 315 K using the leapfrog integrator. Dynamics, with a time step of 2 fs, were propagated in the

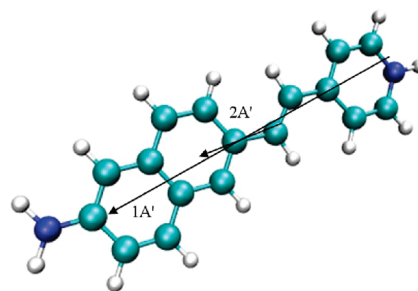


Figure 4. Transition dipole moments of the first two singlet excited states calculated in the gas phase using CASSCF.

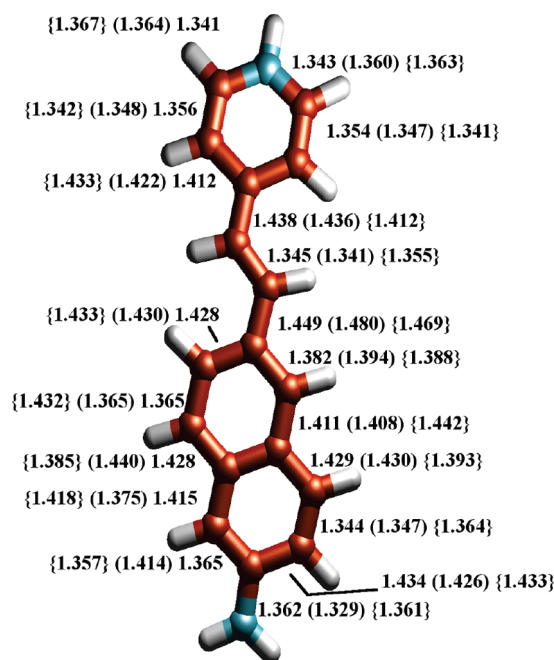


Figure 5. Calculated bond lengths for the ground state, 1A' state (parentheses), and 2A' state (curly brackets) computed at the CASSCF level of theory.

NVE (microcanonical) ensemble. Cubic periodic boundary conditions were imposed throughout. Further equilibration was carried out for 1 ns. Production dynamics were performed for 10 ns. The minimized structure obtained from the pure DPPC system was used as the starting point for the mixed DPPC/cholesterol. On each leaflet, 15 DPPC molecules were replaced by cholesterol, to give a total of 30 cholesterol molecules and 70 DPPC molecules. The simulation then followed the details given above.

TDDFT was used to calculate the vertical absorption energies and emission energies of di-8-ANEPPS in snapshots taken at 50 ps intervals from the last 5 ns of the MD simulations. The reduced model of di-8-ANEPPS shown in Figure 1 was used because this was the smallest portion of the full molecule that reproduced the same vertical excitation spectrum in the gas phase as the full molecule. The emission spectra were generated from MD simulations in which the point charges for the di-8-ANEPPS fluorophore were taken from the excited-state CASSCF simulations; these are available in the Supporting Information. It would be desirable to use a QM/MM scheme to propagate the

excited-state dynamics; however, time scales for such a scheme would be very short, and therefore, the modified force field charges were used as an approximation to the full QM/MM technique. In one set of calculations, the environment was considered as point charges taken from the CHARMM27 force field. The spectra were also computed by including the immediate surrounding environment explicitly in the TDDFT calculation. Lipid, cholesterol, and water molecules were included explicitly in the TDDFT calculation if any of the atoms were within either of two spheres of radius 4.5 Å, centered on the ring-fusing bond of naphthalene and the midpoint of the bond between the carbon atom of the ethene group and the carbon atom of the pyridinium ring (Figure 3a). The number of lipid atoms that this introduced was very large, and therefore, the DPPC and cholesterol molecules were further split (Figure 3b,c), according to the charge groups specified in the CHARMM27 topology files and the condition that one (or more) of the atoms of the subgroup has to be within 4.5 Å of di-8-ANEPPS, as described above. The rest of the membrane environment was included as point charges; where a lipid molecule had been split, the charges of the next group were renormalized so as to give a total system that was charge-neutral. This led to TDDFT calculations with a maximum of 260 atoms and 2325 basis functions.

In order to calculate such large snapshots, a scheme was utilized involving a truncated set of single excitations between the occupied and virtual orbitals associated with the atoms of the fluorophore.⁴⁴ In this scheme, occupied orbitals are chosen based upon their Mulliken populations. If $\{\lambda\}$ is the subset of basis functions centered on the fluorophore atoms, a parameter κ_i^{occ} is

defined such that

$$\kappa_i^{\text{occ}} = \sum_{\lambda} M_{\lambda i} \quad (1)$$

where $M_{\lambda i}$ is the contribution to the Mulliken population of orbital i from basis function λ . κ_i^{occ} is, therefore, a measure of the atoms on which orbital i is localized. Similarly, a parameter κ_a^{vir} can be defined for virtual orbitals, based upon molecular orbital coefficients c

$$\kappa_a^{\text{vir}} = \sum_{\lambda} c_{\lambda a}^2 \quad (2)$$

For this study, an occupied orbital i was included if $\kappa_i^{\text{occ}} \geq 0.4$, and a virtual orbital a was included if $\kappa_a^{\text{vir}} \geq 0.5$. This approach has proven to be successful in previous applications.^{32,33,44–46} The scheme also makes the identification of the states of interest much easier than using a full TDDFT calculation. For this reason, we favored this approach over recent advances in multireference perturbation theory approaches.^{47–49}

It has been speculated that the lowest valence excited states of di-8-ANEPPS are due to charge transfer;²⁵ TDDFT is known to fail for charge-transfer states.⁵⁰ However, there is now a sizable body of work on the modification of the exchange-correlation functional to remedy this.^{51–65} We used Coulomb attenuated or long-range corrected (LRC) DFT, which depends upon a partitioning of the electron repulsion operator into long-range and short-range components, in the evaluation of the exchange energy

$$\frac{1}{r_{12}} = \frac{1 - \text{erf}(\omega r_{12})}{r_{12}} + \frac{\text{erf}(\omega r_{12})}{r_{12}} \quad (3)$$

where erf is the error function and $r_{12} = |\mathbf{r}_1 - \mathbf{r}_2|$. The first term on the right-hand side of eq 3 is the short-range contribution and is evaluated with DFT, while the long-range contribution is treated with Hartree–Fock (HF) exchange. This incorporates long-range HF exchange with standard DFT exchange, providing a correct description at long range. We used the LRC-PBE functional,^{66,67} with $\omega = 0.25 \text{ bohr}^{-1}$. The 6-311G(d) basis set of Pople and co-workers⁶⁸ was used for all atoms.

Table 3. Franck–Condon Vertical Excitation Energy, 0–0 Transition Energy, and Emission Energy of the First Two Singlet Excited States of Di-8-ANEPPS in eV

	CASPT2			TDDFT (LRC-PBE)		
	vertical	0–0	emission	vertical	0–0	emission
1A'	2.67	2.60	2.56	2.87	2.80	2.74
2A'	3.63	3.41	3.14	3.59	3.42	3.13

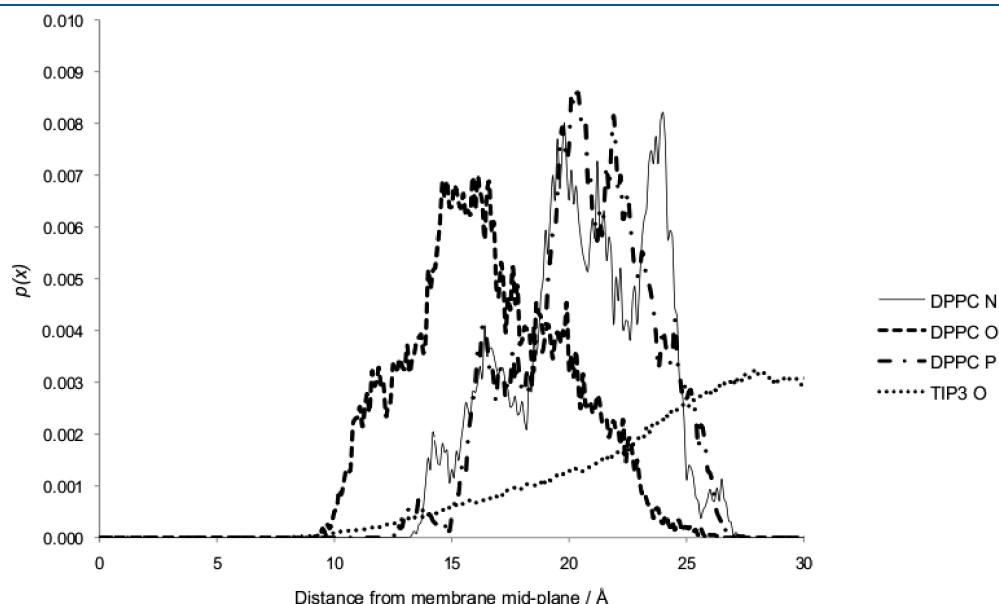


Figure 6. Normalized probability distribution of finding lipid and water atoms in the head group region.

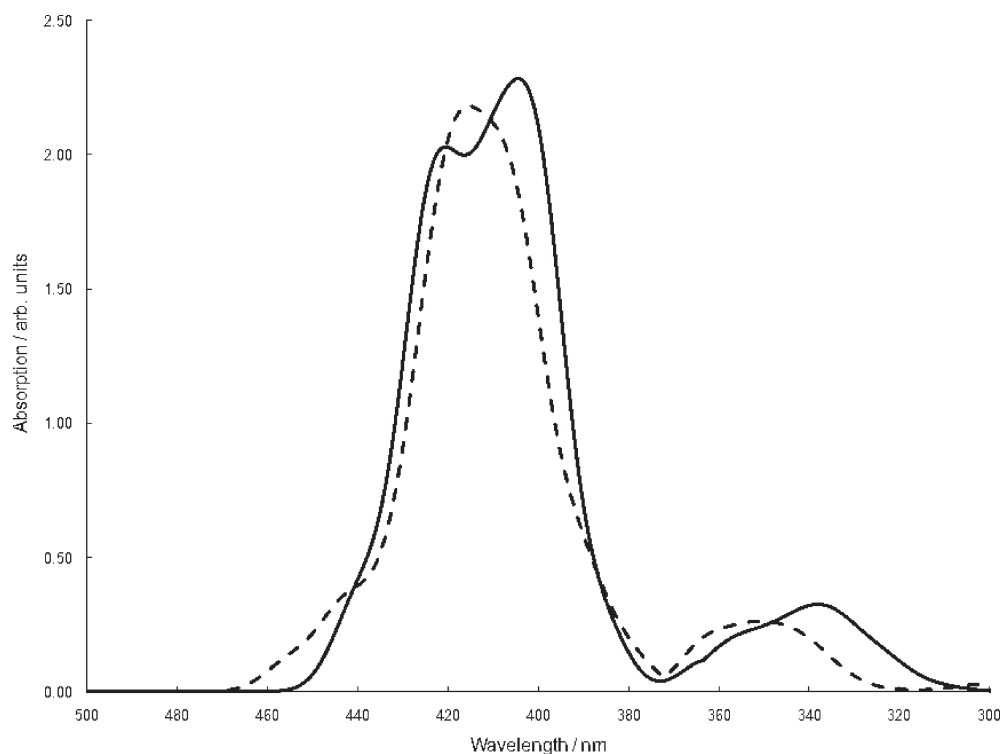


Figure 7. Electronic absorption spectra for di-8-ANEPPS in the DPPC (solid line) and DPPC/cholesterol (dashed line) bilayers.

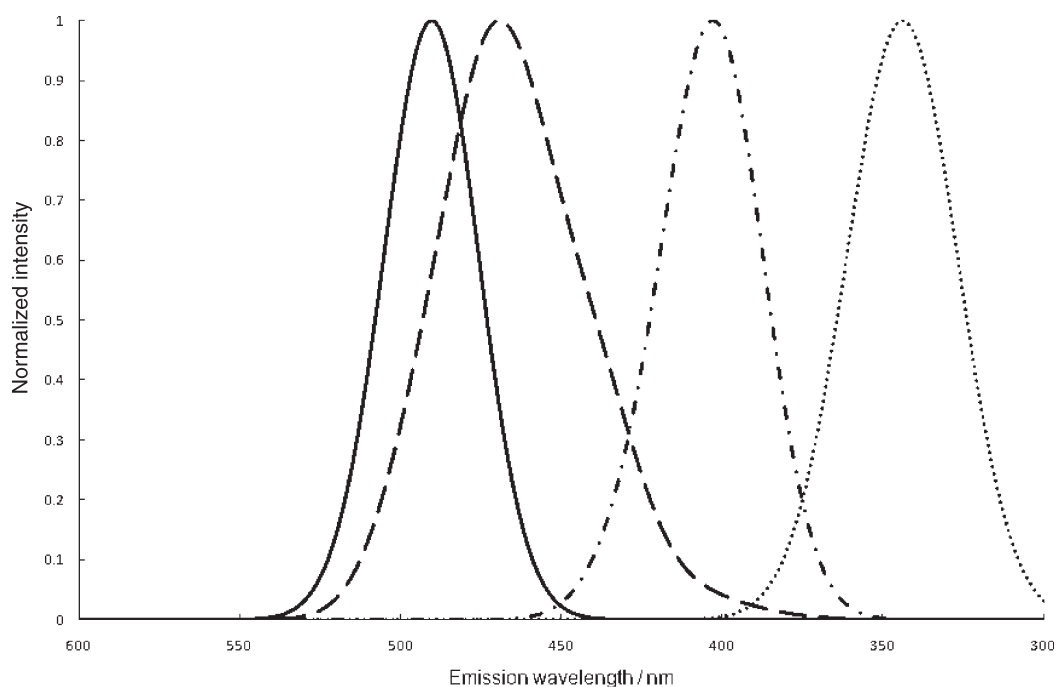


Figure 8. Calculated dual-wavelength emission spectra of di-8-ANEPPS in the pure DPPC and mixed DPPC/cholesterol bilayers. DPPC/cholesterol 1A' (solid line) and 2A' (long dashes). Pure DPPC 1A' (dot-dash) and 2A' (dots).

RESULTS AND DISCUSSION

First, we consider the *ab initio* calculations in the gas phase. The CASSCF CI coefficients and natural orbital occupation numbers for the ground and first two excited states are presented in Tables 1 and 2. The weight of the root determinant at the ground state illustrates that a single-reference description can

correctly describe this state. The first excited state shows a simple charge transfer, which can be well described by single-reference techniques, such as TDDFT, as long as a Coulomb attenuated density functional is used. This state involves excitation of a π -electron from orbital 9a'' on the naphthyl moiety into the 15a'' antibonding orbital localized on the pyridinium moiety. The

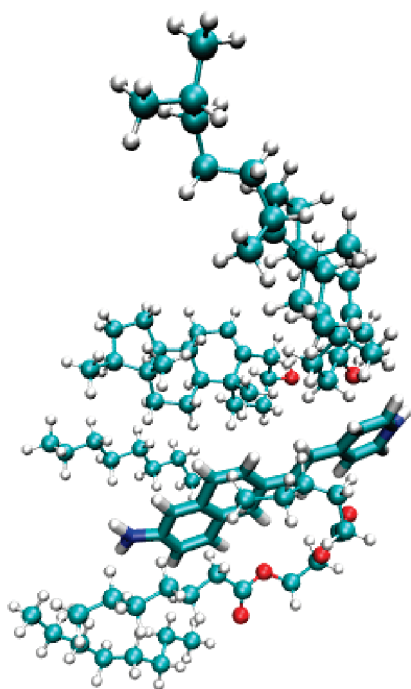


Figure 9. The largest system treated explicitly with TDDFT, containing 260 atoms and using 2325 basis functions. Di-8-ANEPPS is shown as a tubular structure; the explicit environment is shown as a ball-and-stick structure.

second excited state also shows a charge transfer from the pyridinium nitrogen to the naphthyl nitrogen, with the primary excitation from orbital $10a''$ to $15a''$. The determinant with a weight of 23% (Table 1) describes a $\pi \rightarrow \pi^*$ excitation between orbitals $9a''$ and $16a''$ of the naphthyl moiety, which localizes the positive charge from the ring onto the amino nitrogen atom. Figure 4 shows the transition dipole moments and the direction of the charge transfer of the first two excited states of di-8-ANEPPS.

Figure 5 shows the calculated bond lengths of the three electronic states under consideration. The changes in the bond lengths between the ground state and the excited states follow the pattern described by the CASSCF determinants. The N–H bond lengthens upon excitation due to population of the antibonding π^* orbital on the pyridinium moiety. Bond lengths on the naphthyl moiety also increase upon excitation, where the electron density from the π -bonding orbitals shifts to the pyridinium moiety. Table 3 gives the CASPT2 and TDDFT values for the vertical excitation, 0–0 transition, and emission energies for the first two singlet excited states of di-8-ANEPPS. The Coulomb-attenuated scheme is necessary for TDDFT to describe the charge-transfer excitations properly; the standard PBE functional is in error by more than 1 eV for each state. The agreement with CASPT2 results is very good, particularly for the second excited state. The average error for the transitions considered is 0.11 eV, and the largest deviation is 0.20 eV, which is within the accepted accuracy range for TDDFT.⁶⁹

We now turn to the MD simulation. Figure 6 shows the normalized probability function of finding head group boundary atoms. The probability distribution of the atoms within the head group region shows the membrane–water boundary to be quite flexible or fuzzy, having a depth of approximately 10 Å, in accord

with other studies.⁷⁰ The calculated dipole potential difference between the two systems was ~ 70 mV, with the pure DPPC bilayer having the lower potential, in good agreement with experiment. Further characterization of the MD simulations will be presented elsewhere; here, our focus is on how the different explicit molecular environments generated in the MD simulations influence the spectroscopy of di-8-ANEPPS.

The calculated absorption spectra of di-8-ANEPPS in the two bilayer systems are presented in Figure 7. These spectra are computed for conformational ensembles comprising 100 snapshots uniformly sampled from the MD trajectory. Lipid, cholesterol, and water molecules were included explicitly in the TDDFT calculation if any of the atoms were within either of two spheres of radius 4.5 Å (Figure 3). Because there are 130 atoms per DPPC molecule, the lipids were further split according to the groups defined in the CHARMM27 topology files, providing charge-neutral groups (except for the head group components, which had a charge of either +1 or –1). The intensity of the absorption peaks was taken from the calculated oscillator strengths for the conformations sampled. The shift in absorption for each peak is small between the pure DPPC and mixed DPPC/cholesterol bilayer, in agreement with experimental findings. The absorption spectrum shows a very small shift to longer wavelength when the membrane dipole potential is strongest.

The calculated emission spectra are given in Figure 8. The spectra were calculated as a sum of convoluted Gaussian functions with a half-width of 10 nm. Experimentally, the effect of probe concentration causes larger fluorescence shifts than the membrane dipole potential, and therefore, the ratio of the emission intensity of the two excited states is used because this is largely invariant to probe concentration. Because the emission intensity depends on the quantum yield of an emitting species, a quantity which cannot be calculated, we cannot compare directly with experiments in which the dual-wavelength ratiometric measurements are reported. However, we can deduce the causes of the fluorescence shift on each excited state explicitly. The λ_{max} of the two excited states of di-8-ANEPPS in the pure DPPC bilayer are separated by ~ 60 nm. Both states shift to longer wavelength in the DPPC/cholesterol bilayer. The $2A'$ state shows a larger shift than the $1A'$ state, bringing the peaks to just 21 nm apart.

Figure 9 shows the largest snapshot calculated at the TDDFT level, with 260 atoms and 2325 basis functions. The effect of explicit molecular interactions upon the absorption and emission characteristics was investigated. The effect of the intermolecular bond lengths between the nitrogen atoms of di-8-ANEPPS and potential hydrogen-bonding hydrogen atoms of the surrounding lipids and cholesterol upon emission was analyzed first. In all cases, there was no correlation between the geometric parameters and the shifts ($r^2 < 0.1$ in all cases). The effect of the dipole potential on the emission spectra was considered next. Figure 10 shows the average emission energy as a function of the scaling of the point charges in the TDDFT calculations, in which only the di-8-ANEPPS fluorophore was treated explicitly. In this case, unity corresponds to the CHARMM27 force field for the DPPC/cholesterol system, and zero corresponds to the gas-phase TDDFT values (i.e., the point charges are all zero). Larger values correspond to an increase in the membrane dipole potential. The emission energies calculated for each of the first two singlet excited states decreases with increasing scaling of the point charges, thus corresponding to a monotonic relationship with the membrane dipole potential. Scaling the point charges to

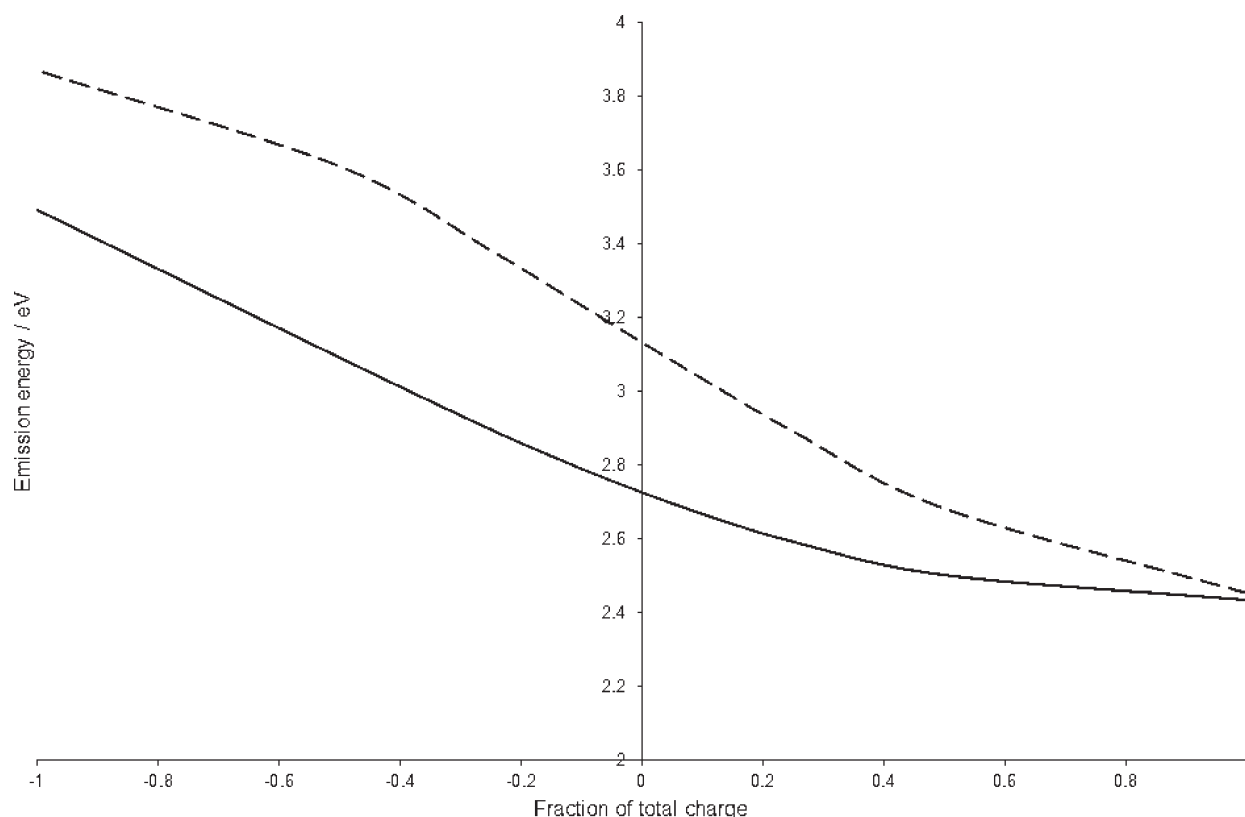


Figure 10. The computed emission energies for the 1A' (solid line) and 2A' (dashed line) states as a function of the scaling of the point charges obtained from the CHARMM27 force field, for TDDFT (LRC-PBE) calculations involving only the di-8-ANEPPS fluorophore and the environment consisting of only point charges. Here, a scale factor of zero corresponds to the gas phase, and a scale factor of 1 corresponds to the CHARMM27 force field values.

higher values than those of the CHARMM27 force field does not lead to any further convergence of the two states. Given that values larger than those given in the force field may lead to unphysical polarization of the electronic wave function, scaling was not considered beyond 1.2. Interestingly, the linear relationship holds for inverted values of the CHARMM27 charges, reaching a maximum in the difference between the two peaks at a scale value of ~ -0.5 . This corresponds to an inverted membrane dipole potential.

CONCLUSIONS

We have studied the effect of the membrane dipole potential and explicit molecular interactions on the emission spectra of di-8-ANEPPS in two different model membrane bilayers. We have also studied the effect of using the second excited state of di-8-ANEPPS as a probe of the membrane dipole potential, which is not currently exploited experimentally. Our findings show that either of the first two excited states could be used as a fast potentiometric probe. The excited-state geometries and the nature of the transitions were determined using gas-phase CASSCF calculations. The condensed-phase emission spectra were determined using a decoupled QM/MM scheme, where snapshots taken from a classical MD simulation were calculated using TDDFT. Many experimental groups have used the fluorescent molecular probe, di-8-ANEPPS, on the assumption that explicit, specific molecular interactions do not affect the emission spectrum. Our findings, based on the experimental work found in ref 19, provide concrete support that this assumption is correct and that the emission shifts observed are due only to changes in the membrane dipole potential. This work should help

experimental groups to use di-8-ANEPPS in more challenging membrane environments with increased confidence, such as membrane rafts, where the density is greater and one would expect stronger molecular interactions.

ASSOCIATED CONTENT

S Supporting Information. Calculated geometrical parameters of truncated di-8-ANEPPS in the ground state and 1A' and 2A' excited states and the CHARMM parameters of di-8-ANEPPS are given. This material is available free of charge via the Internet at <http://pubs.acs.org>.

AUTHOR INFORMATION

Corresponding Author

*E-mail: Jonathan.hirst@nottingham.ac.uk.

ACKNOWLEDGMENT

This work was supported through the Engineering and Physical Sciences Research Council through the award of a grant (EP/F006780/1). D.R. thanks the Leverhulme Trust for an Early Career Fellowship. We thank the University of Nottingham for time on the high-performance computing service.

REFERENCES

- (1) Helms, V. *Curr. Opin. Struct. Biol.* **2002**, *12*, 169–175.
- (2) Paulick, M. G.; Forstner, M. B.; Groves, J. T.; Bertozzi, C. R. *Proc. Natl. Acad. Sci. U.S.A.* **2007**, *104*, 20332–20337.

- (3) Limon, A.; Reyes-Ruiz, J. M.; Eusebi, F.; Miledi, R. *Proc. Natl. Acad. Sci. U.S.A.* **2007**, *104*, 15526–15530.
- (4) Levine, B. G.; Coe, J. D.; Martinez, T. J. *J. Phys. Chem. B* **2008**, *112*, 405–413.
- (5) Leake, M. C.; Chandler, J. H.; Wadhams, G. H.; Bai, F.; Berry, R. M.; Armitage, J. P. *Nature* **2006**, *443*, 355–358.
- (6) Prescott, M.; Battad, J.; Wilmann, P.; Rossjohn, J.; Devenish, R. *Biotechnol. Annu. Rev.* **2006**, *12*, 31–66.
- (7) Zhang, Z.; Alfonta, L.; Tian, F.; Bursulaya, B.; Uryu, S.; King, D. S.; Schultz, P. G. *Proc. Natl. Acad. Sci. U.S.A.* **2004**, *101*, 8882–8887.
- (8) Hogue, C. W. V.; Rashquinha, I.; Szabo, A. G.; MacManus, J. P. *FEBS Lett.* **1992**, *310*, 269–272.
- (9) Ross, J. B. A.; Senear, D. F.; Waxman, E.; Kombo, B. B.; Rusinova, E.; Huang, Y. T.; Laws, W. R.; Hasselbacher, C. A. *Proc. Natl. Acad. Sci. U.S.A.* **1992**, *89*, 12023–12027.
- (10) Botchway, S. W.; Barba, I.; Jordan, R.; Harmston, R.; Haggie, P. M.; William, S. P.; Fulton, A. M.; Parker, A. W.; Brindle, K. M. *Biochem. J.* **2005**, *390*, 787–790.
- (11) Bouevitch, O.; Lewis, A.; Pinevsky, I.; Wuskell, J. P.; Loew, L. M. *Biophys. J.* **1993**, *65*, 672–679.
- (12) Campagnola, P. J.; Wei, M. D.; Lewis, A.; Loew, L. M. *Biophys. J.* **1999**, *77*, 3341–3349.
- (13) Millard, A. C.; Jin, L.; Lewis, A.; Loew, L. M. *Opt. Lett.* **2003**, *28*, 1221–1223.
- (14) Fluhler, E.; Burnham, V. G.; Loew, L. M. *Biochemistry* **1985**, *24*, 5749–5755.
- (15) Zhang, J.; Davidson, R. M.; Wei, M. D.; Loew, L. M. *Biophys. J.* **1998**, *74*, 48–53.
- (16) Loew, L. M. *Pure Appl. Chem.* **1996**, *68*, 1405–1409.
- (17) Millard, A. C.; Jin, L.; Wei, M. D.; Wuskell, J. P.; Lewis, A.; Loew, L. M. *Biophys. J.* **2004**, *86*, 1169–1176.
- (18) Montana, V.; Farkas, D. L.; Loew, L. M. *Biochemistry* **1989**, *28*, 4536–4539.
- (19) Goff, G. L.; Vitha, M. F.; Clarke, R. J. *Biochim. Biophys. Acta* **2007**, *1768*, 562–570.
- (20) Brockman, H. *Chem. Phys. Lipids* **1994**, *73*, 57–79.
- (21) Clarke, R. J. *Biochim. Biophys. Acta* **1997**, *1327*, 269–278.
- (22) Pickar, A. D.; Benz, R. *J. Membr. Biol.* **1978**, *44*, 353–376.
- (23) Gawrisch, K.; Ruston, D.; Zimmerberg, J.; Parsegian, V. A.; Rand, R. P.; Fuller, N. *Biophys. J.* **1992**, *61*, 1213–1223.
- (24) O'Shea, P. Membrane Potentials; measurement, occurrence and roles in cellular function. In *Bioelectrochemistry of Membranes*; Walz, D., et al. Eds.; Birkhauser Verlag: Switzerland, 2004; pp 23–59.
- (25) Rusu, C. F.; Lanig, H.; Othersen, O. G.; Kryschi, C.; Clark, T. *J. Phys. Chem. B* **2008**, *112*, 2445–2455.
- (26) See, for example: Roos, B. O. *Adv. Chem. Phys.* **1987**, *69*, 399–442.
- (27) Andersson, K.; Malmqvist, P.-Å.; Roos, B. O.; Sadlej, A. J.; Wolinski, K. *J. Phys. Chem.* **1990**, *94*, 5483–5488.
- (28) Andersson, K.; Malmqvist, P.-Å.; Roos, B. O. *J. Chem. Phys.* **1992**, *96*, 1218–1226.
- (29) Finley, J.; Malmqvist, P.-Å.; Roos, B. O.; Serrano-Andres, L. *Chem. Phys. Lett.* **1998**, *288*, 299–306.
- (30) Ghigo, G.; Roos, B. O.; Malmqvist, P.-Å. *Chem. Phys. Lett.* **2004**, *396*, 142–149.
- (31) Cossi, M.; Barone, V. *J. Chem. Phys.* **2000**, *112*, 2427–2435.
- (32) Robinson, D.; Besley, N. A.; Lunt, E. A. M.; O'Shea, P.; Hirst, J. D. *J. Phys. Chem. B* **2009**, *113*, 2535–2541.
- (33) Robinson, D.; Besley, N. A.; O'Shea, P.; Hirst, J. D. *J. Phys. Chem. B* **2009**, *113*, 14521–14528.
- (34) Widmark, P.-O.; Malmqvist, P.-Å.; Roos, B. O. *Theor. Chim. Acta* **1990**, *77*, 291–306.
- (35) Malmqvist, P.-Å.; Rendell, A.; Roos, B. O. *J. Phys. Chem.* **1990**, *94*, 5477–5482.
- (36) Karlström, G.; Lindh, R.; Malmqvist, P.-Å.; Roos, B. O.; Ryde, U.; Veryazov, V.; Widmark, P.-O.; Cossi, M.; Schimmelpfennig, B.; Neogrady, P.; Seijo, L. *Comput. Mater. Sci.* **2003**, *28*, 222–239.
- (37) Brooks, B. R.; Bruccoleri, R. E.; Olafson, B. D.; States, D. J.; Swaminathan, S.; Karplus, M. *J. Comput. Chem.* **1983**, *4*, 187–217.
- (38) Feller, S.; MacKerell, A. D., Jr. *J. Phys. Chem. B* **2000**, *104*, 7510–7515.
- (39) Krol, M.; Borowski, T.; Roterman, I.; Piekarska, B.; Stopa, B.; Rybarska, J.; Konieczny, L. *J. Comput.-Aided Mol. Des.* **2004**, *18*, 41–53.
- (40) Yin, D. *Parameterization for Empirical Force Field Calculations and A Theoretical Study of Membrane Permeability of Pyridine Derivative*. Ph.D. Thesis, Department of Pharmaceutical Sciences, School of Pharmacy, University of Maryland, 1997.
- (41) Jorgensen, W. L.; Chandrasekhar, J.; Madura, D.; Impey, R. W.; Klein, M. L. *J. Chem. Phys.* **1983**, *79*, 926–935.
- (42) Ryckaert, J.-P.; Ciccotti, G.; Berendsen, H. J. C. *J. Comput. Phys.* **1977**, *23*, 327–341.
- (43) Darden, T.; York, D.; Pederson, L. *J. Chem. Phys.* **1993**, *98*, 10089–10092.
- (44) Besley, N. A. *Chem. Phys. Lett.* **2004**, *390*, 124–129.
- (45) Besley, N. A.; Oakley, M. T.; Cowan, A. J.; Hirst, J. D. *J. Am. Chem. Soc.* **2004**, *126*, 13502–13511.
- (46) Besley, N. A.; Blundy, A. J. *J. Phys. Chem. B* **2006**, *110*, 1701–1710.
- (47) Potts, D. M.; Taylor, C. M.; Chaudhuri, R. K.; Freed, K. F. *J. Chem. Phys.* **2001**, *114*, 2592–2600.
- (48) Aquilante, F.; Malmqvist, P.-Å.; Pedersen, T. B.; Ghosh, A.; Roos, B. O. *J. Chem. Theory Comput.* **2008**, *4*, 694–702.
- (49) Robinson, D.; McDouall, J. J. W. *J. Phys. Chem. A* **2007**, *111*, 9815–9822.
- (50) Dreuw, A.; Weisman, J. L.; Head-Gordon, M. *J. Chem. Phys.* **2003**, *119*, 2943–2946.
- (51) Tozer, D. J. *J. Chem. Phys.* **2003**, *119*, 12697–12699.
- (52) Gill, P. M. W.; Adamson, R. D.; Pople, J. A. *Mol. Phys.* **1996**, *88*, 1005–1009.
- (53) Leininger, T.; Stoll, H.; Werner, H. J.; Savin, A. *Chem. Phys. Lett.* **1997**, *275*, 151–160.
- (54) Iikura, H.; Tsuneda, T.; Yanai, T.; Hirao, K. *J. Chem. Phys.* **2001**, *115*, 3540–3544.
- (55) Heyd, J.; Scuseria, G. E.; Ernzerhof, M. *J. Chem. Phys.* **2003**, *118*, 8207–8215.
- (56) Tawada, Y.; Tsuneda, T.; Yanagisawa, S.; Yanai, T.; Hirao, K. *J. Chem. Phys.* **2004**, *120*, 8425–8433.
- (57) Toulouse, J.; Colonna, F.; Savin, A. *Phys. Rev. A* **2004**, *70*, 062505.
- (58) Yanai, T.; Tew, D. P.; Handy, N. C. *Chem. Phys. Lett.* **2004**, *393*, 51–57.
- (59) Kamiya, M.; Sekino, H.; Tsuneda, T.; Hirao, K. *J. Chem. Phys.* **2005**, *122*, 234111.
- (60) Sato, T.; Tsuneda, T.; Hirao, K. *Mol. Phys.* **2005**, *103*, 1151–1164.
- (61) Yanai, T.; Harrison, R. J.; Handy, N. C. *Mol. Phys.* **2005**, *103*, 413–424.
- (62) Vydrov, O. A.; Heyd, J.; Krukau, A. V.; Scuseria, G. E. *J. Chem. Phys.* **2006**, *125*, 074106.
- (63) Vydrov, O. A.; Scuseria, G. E. *J. Chem. Phys.* **2006**, *125*, 234109.
- (64) Henderson, T. M.; Izmaylov, A. F.; Scuseria, G. E.; Savin, A. *J. Chem. Phys.* **2007**, *127*, 221103.
- (65) Henderson, T. M.; Janesko, B. G.; Scuseria, G. E. *J. Chem. Phys.* **2008**, *128*, 194105.
- (66) Perdew, J. P.; Burke, K.; Ernzerhof, M. *Phys. Rev. Lett.* **1996**, *77*, 3865–3868.
- (67) Rohrdanz, M. A.; Martins, K. M.; Herbert, J. M. *J. Chem. Phys.* **2009**, *130*, 054112.
- (68) Krishnan, R.; Binkley, J. S.; Seeger, R.; Pople, J. A. *J. Chem. Phys.* **1980**, *72*, 650–654.
- (69) Tozer, D. J.; Amos, R. D.; Handy, N. C.; Roos, B. O.; Serrano-Andres, L. *Mol. Phys.* **1999**, *97*, 859–868.
- (70) Woolf, T. B.; Roux, B. *Proc. Natl. Acad. Sci. U.S.A.* **1994**, *91*, 11631–11635.